ACS ORGANIC & INORGANIC Au
AN OPEN ACCESS JOURNAL OF THE AMERICAN CHEMICAL SOCIETY

pubs.acs.org/orginorgau

Article

Influence of the CH/B replacement on the Reactivity of Boranthrene and Related Compounds

Iván Cortés, Jorge Juan Cabrera-Trujillo, and Israel Fernández*

Cite This: *ACS Org. Inorg. Au* 2022, 2, 44–52

Read Online

ACCESS | Metrics & More | Article Recommendations | Supporting Information

ABSTRACT: The influence of the replacement of CH groups by boron atoms on the reactivity of planar polycyclic aromatic hydrocarbons has been explored by means of computational tools. To this end, [4 + 2]-cycloaddition reactions involving anthracene and neutral boranthrene with different dienophiles such as ethylene, acetylene, and CO_2 have been compared. In addition, the influence of additional fused aromatic rings (pentacene or borapentacene) on the reactivity of these species has been also explored. It was found that the B-doped systems are systematically much more reactive than their all-carbon counterparts from both kinetic and thermodynamic points of view. The observed trends in reactivity are quantitatively analyzed in detail using state-of-the-art methods, namely, the activation strain model of reactivity and the energy decomposition analysis method. Our calculations reveal the importance of molecular orbital interactions as the key factor responsible for the enhanced reactivity of the B-doped systems.

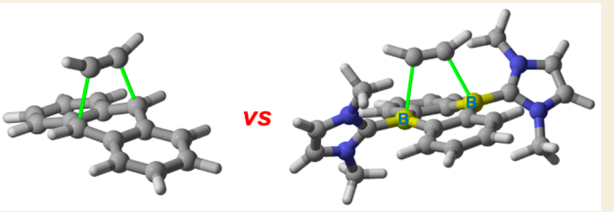

KEYWORDS: *boranthrene, anthracene, reactivity, density functional theory calculations, cycloaddition*

INTRODUCTION

The chemistry of polycyclic aromatic hydrocarbons (PAHs) has experienced a remarkable development in the last decades, which is mainly due to the number of applications of these species in materials science.[1−4] For instance, PAHs have been successfully applied to the design of electronic devices such as organic light-emitting diodes (OLEDs),[5−9] organic field-effect transistors (OFETs),[10−13] and organic photovoltaic cells (OPVs).[14−16]

Despite that, purely organic compounds (i.e., composed exclusively of carbon and hydrogen atoms) do not typically exhibit small band gaps or low-lying LUMO energies and often suffer from other shortcomings such as O_2 sensitivity[17] or self-dimerization (via Diels−Alder reaction),[4,18] severely limiting their applicability. To overcome these disadvantages and modulate the properties of these species, the incorporation of heteroatoms, especially those belonging to groups 13−15, into the framework of PAHs has emerged as a powerful strategy.[19−21] Such C/heteroatom replacement usually has a dramatic impact on the electronic properties of the system, leading to doped PAHs that have applications in materials science as well as medicinal chemistry.[19−21]

In this regard, the integration of boron atoms in doped PAHs is particularly attractive as it has proven to lead to high electron affinities and intense tunable luminescence.[22−26] This can be mainly ascribed to the interaction of the empty p atomic orbital of boron with the surrounding π-system. For instance, 9,10-dihydro-9,10-diboraanthracene (DBA) systems and the corresponding dianion $[DBA]^{2-}$, which have been profusely studied by Wagner and co-workers, should be especially highlighted (Figure 1a).[27−31] Recently, Harman and co-workers prepared and fully characterized the first neutral 1,4-diboron acene homologue, the 9,10-diboraanthracene **1** (also known as boranthrene, Figure 1b).[32] This N-heterocyclic carbene (NHC)-stabilized species features properties typically found in transition metal complexes, such as redox chemistry at mild potentials and a reactivity with small molecule substrates. For instance, **1** is able to react with ethylene and CO_2 to afford the corresponding adducts under relatively mild reaction conditions (Figure 1b). This sharply contrasts with the reactivity of the parent anthracene that, for instance, cannot undergo the analogous reaction with CO_2.

Therefore, it becomes evident that the replacement of carbon atoms by boron atoms in anthracene results in a dramatic reactivity enhancement. Despite that, the factors governing the reactivity enhancement upon the integration of boron atoms in the PAH framework are so far not fully understood. This is crucial because a detailed understanding of the reactivity of these B-doped PAHs may be helpful toward the rational design of novel B-embedded PAH derivatives with different or improved properties. For this reason, in this work we decided to computationally explore the influence of the CH/B replacement on the reactivity of anthracene and related

Received: August 15, 2021
Revised: September 23, 2021
Accepted: September 23, 2021
Published: October 6, 2021

https://doi.org/10.1021/acsorginorgau.1c00023
ACS Org. Inorg. Au 2022, 2, 44–52

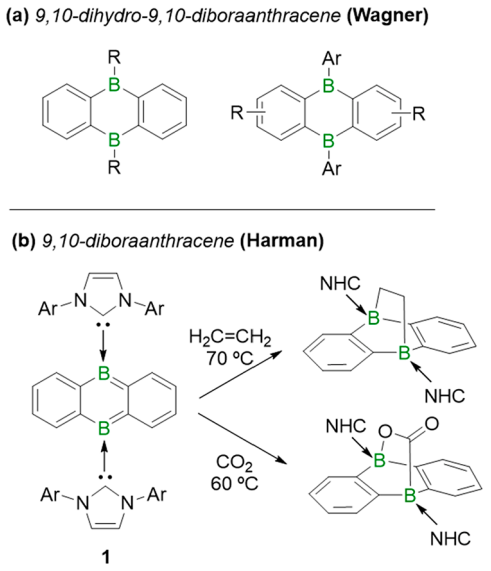

Figure 1. Representative boranthrenes described so far.

larger analogues. To this end, we shall compare the reactions of anthracene and boranthrene with ethylene, acetylene, and CO_2. The trends of reactivity will be quantitatively analyzed using state-of-the-art computational methods, namely, the combination of the activation strain model (ASM)[33−36] of reactivity and the energy decomposition analysis (EDA) method.[37−39] This computational approach has been selected because it has been really useful in rationalizing fundamental processes in organic, organometallic, and main-group chemistry[33−36,40−46] and, in particular, because it has allowed us to understand the reactivity of both planar and curved PAHs, including heteroatom-doped systems.[47−52]

COMPUTATIONAL DETAILS

Geometry optimizations of the molecules were performed without symmetry constraints using the Gaussian 09 (rev. D.01)[53] suite of programs at the dispersion-corrected B3LYP[54−56]-D3[57]/def2-SVP[58,59] level. Reactants and adducts were characterized by frequency calculations and had positive definite Hessian matrices. Transition states (TS's) showed only one negative eigenvalue in their diagonalized force constant matrices, and their associated eigenvectors were confirmed to correspond to the motion along the reaction coordinate under consideration using the intrinsic reaction coordinate (IRC) method.[60] Energy refinements were carried out through single-point calculations at the same DFT level with the much larger triple-ζ basis-set def2-TZVPP[58,59] and including solvent effects (benzene as the solvent) by means of the polarization continuum model (PCM) method.[61−63] This level is denoted PCM(benzene)-B3LYP-D3/def2-TZVPP//B3LYP-D3/def2-SVP.

Activation Strain Model of Reactivity and Energy Decomposition Analysis

The ASM method,[33−36] also known as the distortion and interaction model,[34] involves decomposing the electronic energy (ΔE) into two contributions, namely, the strain or distortion (ΔE_{strain}) that results from the deformation of the individual reactants from their equilibrium geometries and the interaction (ΔE_{int}) between these increasingly deformed reactants along the reaction, ζ, as follows:

$$\Delta E(\zeta) = \Delta E_{strain}(\zeta) + \Delta E_{int}(\zeta)$$

Herein, the reaction coordinate is defined as the projection of the IRC onto the C···C or B···C bond-forming distance.

The EDA method[37−39] is used to further decompose the interaction energy into four energy terms that are associated with the following physical factors: the classical electrostatic interaction between the unperturbed charge distributions of the deformed reactants (ΔE_{elstat}); the destabilizing Pauli repulsion (ΔE_{Pauli}) between closed-shell orbitals; the stabilizing orbital attractions (ΔE_{orb}) that accounts for bond-pair formation, charge transfer (including, among others, HOMO−LUMO interactions), and polarization; and finally interactions coming from dispersion forces (ΔE_{disp}).

$$\Delta E_{int}(\zeta) = \Delta E_{elstat}(\zeta) + \Delta E_{Pauli}(\zeta) + \Delta E_{orb}(\zeta) + \Delta E_{disp}(\zeta)$$

Moreover, the ΔE_{orb} term can be further decomposed by means of the NOCV (natural orbital for chemical valence)[64] extension of the EDA method. The EDA-NOCV approach provides pairwise energy contributions for each pair of interacting orbitals to the total bond energy.

The ADF[65,66] program package was used for EDA calculations using the optimized B3LYP-D3/def2-SVP geometries at the same DFT level in conjunction with a triple-ζ-quality basis set using uncontracted Slater-type orbitals (STOs), which was augmented by two sets of polarization functions with a frozen-core approximation for the core electrons.[67] Auxiliary sets of s, p, d, f, and g STOs were used to fit the molecular densities and represent the Coulomb and exchange potentials accurately in each SCF cycle.[68] Scalar relativistic effects were incorporated by applying the zero-order regular approximation (ZORA).[69−71] This level of theory is denoted ZORA-B3LYP-D3/TZ2P//B3LYP-D3/def2-SVP.

RESULTS AND DISCUSSION

We first focused on the [4 + 2]-cycloaddition reaction of anthracene and boranthrene with ethylene. To this end, we selected three different NHCs, namely, the model 1,3-dimethyl-imidazol-2-ylidene (**1a**), 1,3-diphenyl-imidazol-2-ylidene (**1b**), and the real system with the IPr (1,3-bis(2,6-diisopropylphenyl)imidazol-2-ylidene) NHC (**1c**). Our calculations indicate that the cycloaddition reaction occurs in all cases concertedly through a highly synchronous six-membered transition state (TS), resulting in the corresponding cycloadduct in an exergonic reaction (see Figure 2 for the representative reaction involving **1a**).

Table 1 gathers the computed barrier and reaction energies for all the considered cycloaddition reactions. From the data in Figure 2 and Table 1, it is evident that the processes involving boranthrenes **1a−1c** proceed with a much lower activation barrier ($\Delta\Delta G^{\neq}$ ∼10 kcal/mol)[72] and are much more exergonic. This result nicely agrees with the reactivity enhancement upon the CH/B replacement, as noted above. A similar reactivity trend was found when acetylene was considered as the dienophile (for the corresponding reaction profile, see Figure S1 in the Supporting Information). Moreover, the effect of the substituent directly attached to the nitrogen atoms of the NHC can be considered negligible in view of the rather similar barrier energies computed for the processes involving **1a−1c**. Therefore, the model boranthrene

https://doi.org/10.1021/acsorginorgau.1c00023
ACS Org. Inorg. Au 2022, 2, 44−52

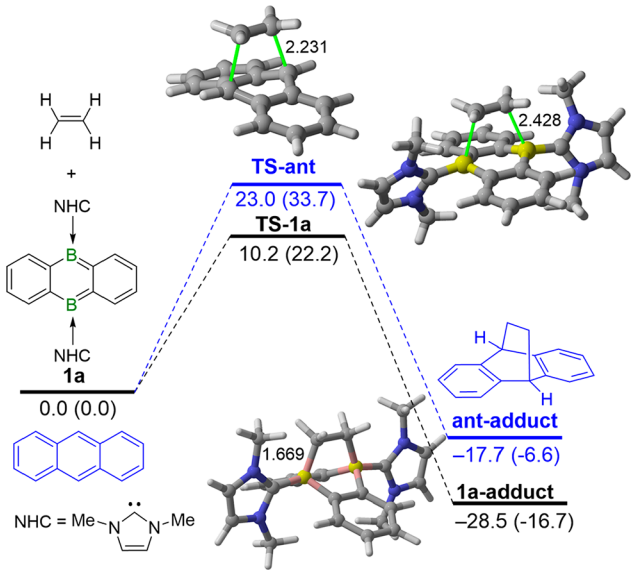

Figure 2. Computed reaction profiles for the cycloaddition reaction involving anthracene (blue lines) and boranthrene **1a** (black lines) with ethylene. Relative energies (free energies, computed at 298 K, within parentheses) and bond distances are given in kcal/mol and angstroms, respectively. All data have been computed at the PCM(benzene)-B3LYP-D3/def2-TZVPP//B3LYP-D3/def2-SVP level.

Table 1. Computed Activation Barriers ($\Delta E^{\neq}$, kcal/mol)[a] and Reaction Energies (ΔE_R, kcal/mol)[b] for the Cycloaddition Reactions Involving Anthracene and Boranthrenes 1a−1c[c]

reaction of anthracene or **1** and ethylene or acetylene		
$\Delta E^{\neq}$	$\Delta E^{\neq}$ ($\Delta G^{\neq}$)	ΔE_R (ΔG_R)
anthracene	23.0 (33.7)	−17.7 (−6.6)
	[27.1 (36.8)][d]	[−27.2 (−17.0)][d]
1a	10.2 (22.2)	−28.5 (−16.7)
	[13.0 (23.8)][d]	[−43.1 (−32.4)][d]
1b	10.0 (23.1)	−23.6 (−9.2)
1c	12.9 (22.6)	−22.5 (−11.7)

[a]Computed as $\Delta E^{\neq}$ = E(TS) − E(diene) − E(dienophile). [b]Computed as ΔE_R = E(cycloadduct) − E(diene) − E(dienophile). [c]Free energies, computed at 298 K, are given within parentheses. [d]Reaction involving acetylene as the dienophile. All data have been computed at the PCM(benzene)-B3LYP-D3/def2-TZVPP//B3LYP-D3/def2-SVP level.

1a can be safely used to find the origin of the computed reactivity trends (see below).

The activation strain model (ASM) of reactivity was then used to quantitatively understand the factors behind the significantly enhanced reactivity of boranthrene. Figure 3 shows the corresponding activation strain diagrams (ASDs) from the initial stages of the transformation up to the corresponding transition states projected onto the C···C (for the process involving anthracene) or B···C (for the process involving boranthrene **1a**) bond-forming distance. The computed ASDs are rather similar for both reactions in the sense that the ΔE_{int} term remains constant or even slightly destabilizing at the initial stages of the transformation but becomes highly stabilizing at the proximity of the transition state. This is the typical behavior that has been observed for analogous [4 + 2]-cycloadditions and related pericyclic

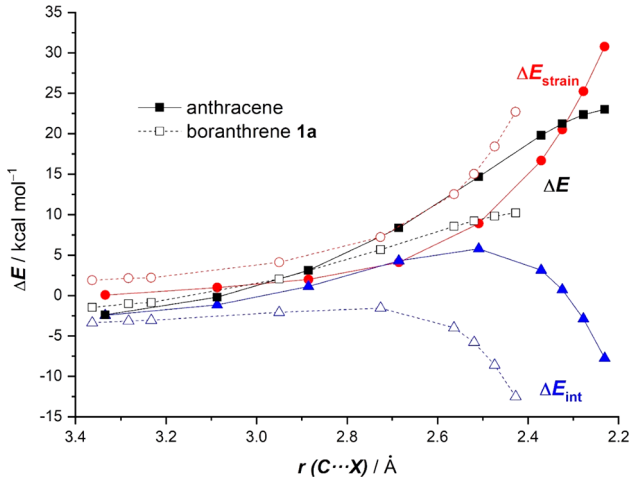

Figure 3. Comparative activation strain analyses of the cycloaddition reactions between ethylene and anthracene (solid lines) or boranthrene **1a** (dashed lines) projected onto the C···C or C···B bond-forming distance, respectively. All data have been computed at the PCM(benzene)-B3LYP-D3/def2-TZVPP//B3LYP-D3/def2-SVP level.

reactions.[47−52,73,74] Despite that, the strain energy (measured by the ΔE_{strain} term) is more destabilizing for the reaction involving **1a** and therefore it is not responsible for the lower barrier computed for the **1a** and ethylene reaction. In contrast, the interaction energy (ΔE_{int}) is clearly much more stabilizing for the boranthrene reaction along the entire transformation. Therefore, it can be concluded that the enhanced reactivity of the B-doped anthracene is solely derived from a strong interaction between the deformed reactants along the entire reaction coordinate.

The energy decomposition analysis (EDA) method was applied next to quantitatively unveil the factors leading to the enhanced interaction computed for the process involving **1a**. As graphically shown in Figure 4, which once again presents the evolution of the EDA terms along the reaction pathway

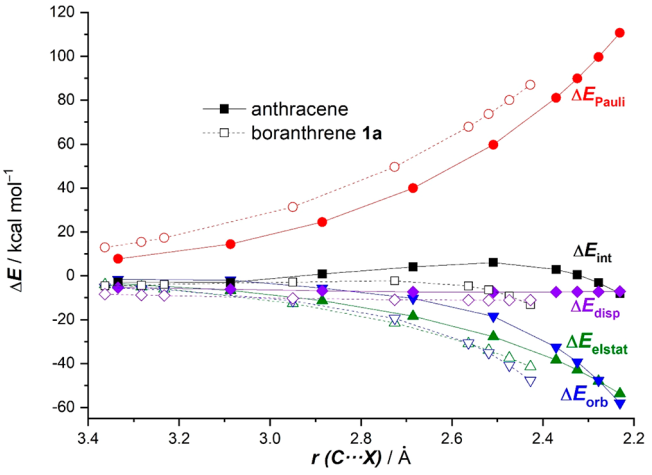

Figure 4. Comparative energy decomposition analyses of the cycloaddition reactions between ethylene and anthracene (solid lines) or boranthrene **1a** (dashed lines) projected onto the C···C or C···B bond-forming distance, respectively. All data have been computed at the ZORA-B3LYP-D3/TZ2P//B3LYP-D3/def2-SVP level.

https://doi.org/10.1021/acsorginorgau.1c00023
ACS Org. Inorg. Au 2022, 2, 44−52

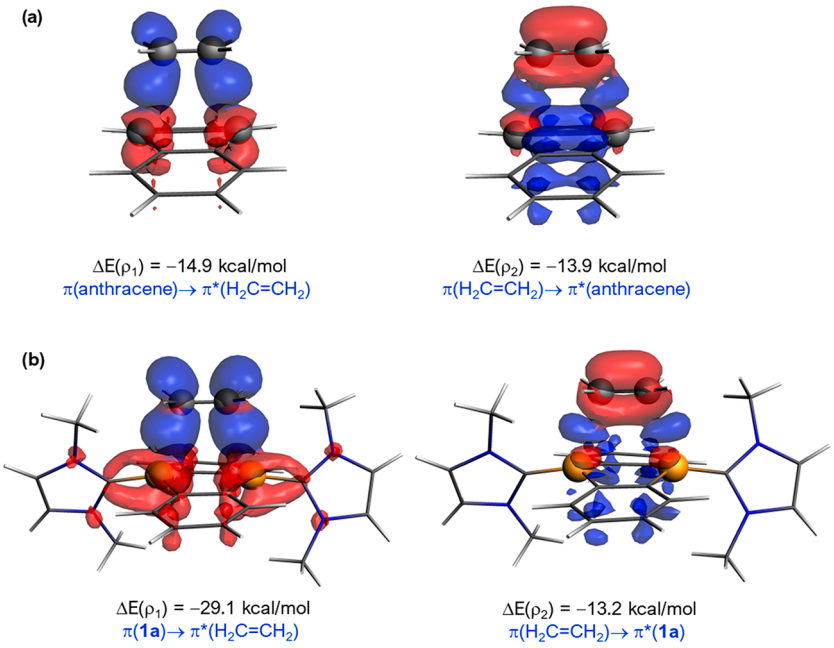

Figure 5. Contour plots of NOCV deformation densities $\Delta\rho$ and associated energies $\Delta E(\rho)$ (computed at the ZORA-B3LYP-D3/TZ2P//B3LYP-D3/def2-SVP level) for the (a) anthracene and ethylene and (b) boranthrene **1a** and ethylene reactions computed at the same consistent C···C and C···B bond-forming distance, respectively, of ca. 2.4 Å. The electron-density charge flows in the red → blue direction.

from the initial stages of the process to the corresponding transition states, all the stabilizing contributions (ΔE_{elstat}, ΔE_{orb}, and ΔE_{disp}) become more stabilizing for the process involving **1a**. These stabilizing contributions compensate for the clearly more destabilizing Pauli repulsion computed for the **1a** and ethylene cycloaddition and therefore this process presents a stronger interaction between the deformed reactants along the cycloaddition reaction as compared to analogous process involving the parent anthracene.

According to the data in Figure 4, the major contribution to the interaction energy difference between both reactions comes from the ΔE_{orb} term,[75] which becomes much more stabilizing for the reaction involving the boranthrene **1a**. This can be initially ascribed to the much lower HOMO(**1a**)−LUMO(ethylene) gap as a consequence of the presence of the boron atoms, which significantly raises the energy of the HOMO(π) from −5.48 eV in anthracene to −2.80 eV in **1a**. To gain a deeper insight into the origin of the crucial ΔE_{orb} term, the natural orbital for chemical valence (NOCV) extension of the EDA method was applied next. This approach identifies two key molecular orbital interactions that govern the total orbital interactions in the considered cycloaddition reactions, namely, the normal electron demand HOMO(π-diene) → LUMO(π*-ethylene) and the inverse electron demand HOMO(π-ethylene) → LUMO(π*-diene) interactions (denoted ρ_1 and ρ_2, respectively; see Figure 5). While the inverse ρ_2 interaction is rather similar for both processes ($\Delta\Delta E(\rho_2)$ = 0.7 kcal/mol, computed at the same consistent C···C or C···B bond-forming distance of ca. 2.4 Å),[76] the normal HOMO(π-diene) → LUMO(π*-ethylene) is markedly stronger in the process involving the boranthrene **1a** ($\Delta\Delta E(\rho_1)$ = 14.2 kcal/mol), which is consistent with the more favorable HOMO(diene)−LUMO(ethylene) gap (see above). Therefore, it can be concluded that the enhanced reactivity of boranthrenes **1**, in comparison with that of anthracene, is mainly derived from a much more stabilizing HOMO(π-diene) → LUMO(π*-ethylene) molecular orbital interaction, which significantly enhances the total interaction between the reactants along the transformation and ultimately leads to a lower activation barrier.

The enhanced reactivity of boranthrene compared to anthracene becomes even more evident when comparing the reactions with carbon dioxide. Once again, both transformations are concerted and proceed through the corresponding six-membered transition state **TS(CO$_2$)**, which on this occasion is highly asynchronous (i.e., the C···C or B···C bond forms ahead of the C···O or B···O bond; see Figure 6). Despite that, the computed reaction profiles clearly confirm that while the reaction involving anthracene is unfeasible in view of its rather high barrier ($\Delta G^{\neq}$ > 50 kcal/mol) and endergonicity (ΔG_R = +35.3 kcal/mol), the reaction involving boranthrene **1a** is both kinetically ($\Delta G^{\neq}$ = 11.6 kcal/mol) and thermodynamically (ΔG_R = −12.2 kcal/mol) much more favorable, which nicely agrees with the experimental observations.

We once again applied the ASM-EDA method to quantitatively rationalize the dramatic difference in reactivity between boranthrene and anthracene when reacting with CO_2. Not surprisingly, the ASM method confirms that despite the strain energy being comparatively more destabilizing for this process as compared to the ethylene reaction,[77] the enhanced reactivity of **1a** is solely derived from a much more stabilizing interaction energy between the deformed reactants along the entire transformation (Figure 7a). Similar to the reaction with ethylene, this stronger interaction originates, according to the EDA method (Figure 7b), from more stabilizing dispersion interactions (ΔE_{disp}), electrostatic attractions (ΔE_{elstat}), and orbital interactions (ΔE_{orb}), the latter of which contributes to a much greater extent.

The crucial role of the orbital interactions is again related to the reduced HOMO(π-diene)−LUMO(π*-CO_2) gap as a consequence of the destabilization of the HOMO in

https://doi.org/10.1021/acsorginorgau.1c00023
ACS Org. Inorg. Au 2022, 2, 44−52

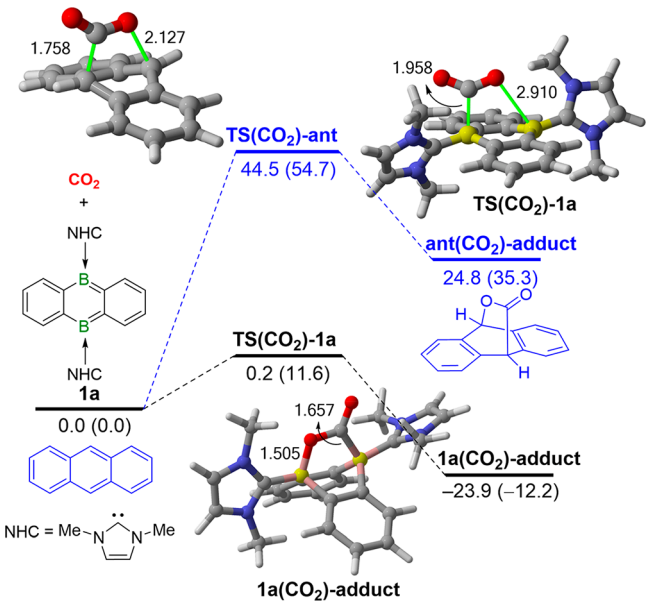

Figure 6. Computed reaction profiles for the cycloaddition reaction involving anthracene (blue lines) and boranthrene **1a** (black lines) with CO_2. Relative energies (free energies, computed at 298 K, within parentheses) and bond distances are given in kcal/mol and angstroms, respectively. All data have been computed at the PCM(benzene)-B3LYP-D3/def2-TZVPP//B3LYP-D3/def2-SVP level.

boranthrene (see above). The NOCV extension of the EDA method confirms that, on this occasion, the main contribution to the total ΔE_{orb} term indeed comes from the HOMO(π-diene) → LUMO(π^*-CO_2) molecular orbital interaction (see Figure 8), which contributes ca. 80−90% to the total orbital interactions. From the data in Figure 8, which shows the corresponding stabilization energies ($\Delta E(\rho_1)$) computed at the same consistent C···C or C···B bond-forming distance of 2.0 Å, the HOMO(**1a**) → LUMO(π^*-CO_2) molecular orbital interaction is significantly higher than the corresponding orbital interaction involving the parent anthracene. This results into a much stronger total interaction between the reactants, which is then reflected in the much lower activation barrier computed for the **1a** and CO_2 reaction.

It is well known that the Diels−Alder reactivity in planar (all carbon) acenes increases with the number of fused rings.[78] This has been traditionally ascribed to the relative stability of the final cycloadducts and not the aromaticity of the reactive ring, which actually becomes the most aromatic ring in all cases. We were finally curious to explore whether this reactivity trend is also followed by the considered B-doped PAHs. To this end, we explored the [4 + 2]-cycloaddition reaction involving ethylene and pentacene and its B-doped counterpart **2a**, where the boron atoms are attached to the model NHC 1,3-dimethyl-imidazol-2-ylidene.

From the data in Figure 9, a similar reactivity enhancement to that observed when comparing anthracene and boranthrene (see above) was found when comparing pentacene and **2a**. Again, the barrier associated with the concerted (and synchronous) [4 + 2]-cycloaddition is ca. 10 kcal/mol lower for the cycloaddition involving **2a**, and the transformation is ca. 10 kcal/mol more exergonic. In addition, and in agreement with the reactivity trend of planar acenes noted above, it was confirmed that the cycloaddition becomes both kinetically (by ca. 4−5 kcal/mol) and thermodynamically (by ca. 12 kcal/mol) more favored with the increasing size of the system. The reduction barrier seems to be directly related to the higher stability of the final cycloadducts. Moreover, the corresponding transition states are reached earlier in the processes involving pentacene and **2a** (bond-forming distances of 2.292 and 2.490 Å, respectively) as compared to the analogous reactions involving their smaller counterparts anthracene and **1a** (bond-forming distances of 2.231 and 2.428 Å, respectively), which is fully consistent with the Hammond−Leffler postulate.[79,80] Indeed, a very good linear relationship was found when the bond-forming distances were plotted versus the computed free activation barriers (correlation coefficient R^2 = 0.99, see Figure S3 in the Supporting Information).

The enhanced reactivity of **2a** as compared to that of pentacene has, according to the ASM-EDA method, the same origin as that found when comparing anthracene and boranthrene. As shown in Figures S4 and S5 in the Supporting

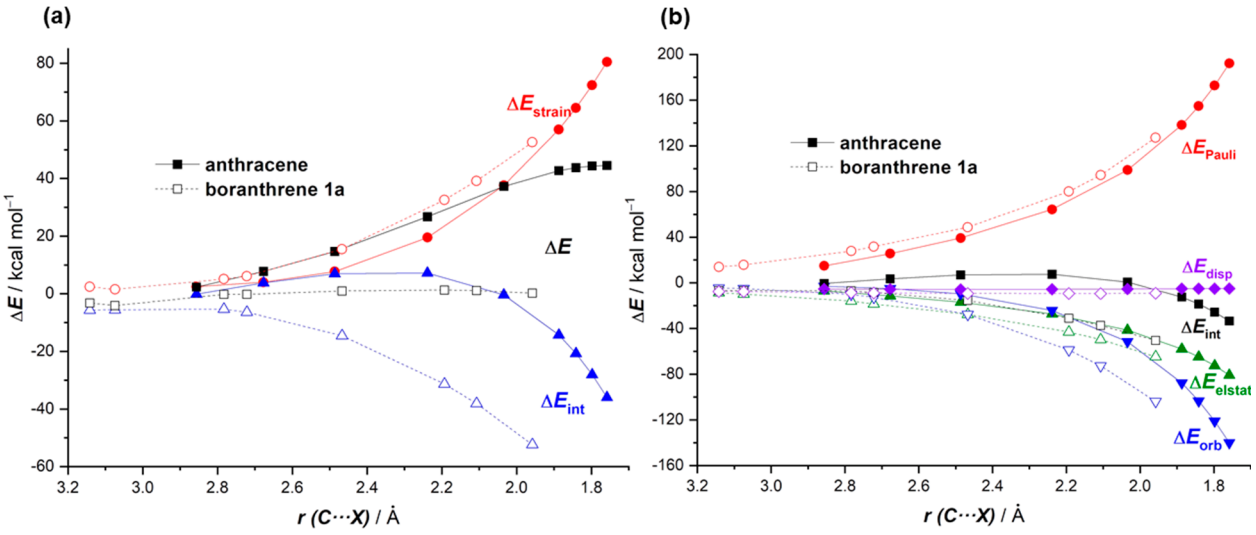

Figure 7. (a) Comparative activation strain and (b) energy decomposition analyses of the cycloaddition reactions between CO_2 and anthracene (solid lines) or boranthrene **1a** (dashed lines) projected onto the C···C or C···B bond-forming distance, respectively.

https://doi.org/10.1021/acsorginorgau.1c00023
ACS Org. Inorg. Au 2022, 2, 44−52

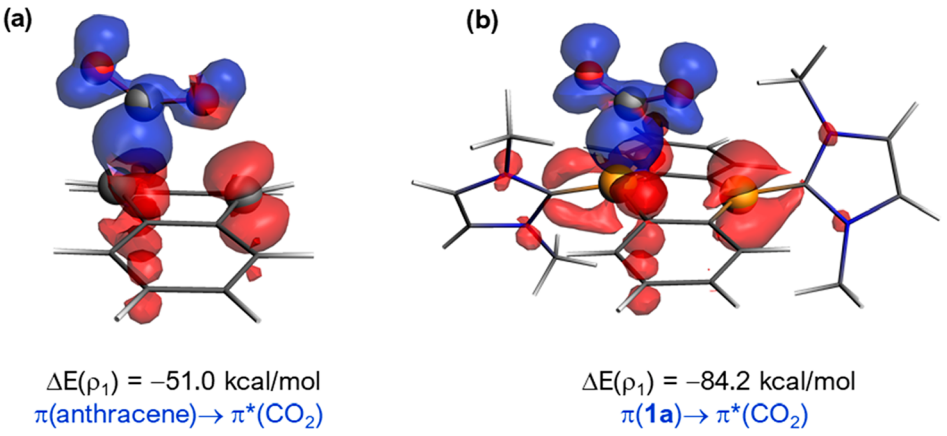

Figure 8. Contour plots of NOCV deformation densities $\Delta\rho$ and associated energies $\Delta E(\rho)$ (computed at the ZORA-B3LYP-D3/TZ2P//B3LYP-D3/def2-SVP level) for the (a) anthracene and CO_2 and (b) boranthrene **1a** and CO_2 reactions computed at the same consistent C···C and C···B bond-forming distance, respectively, of ca. 2.0 Å. The electron-density charge flows in the red → blue direction.

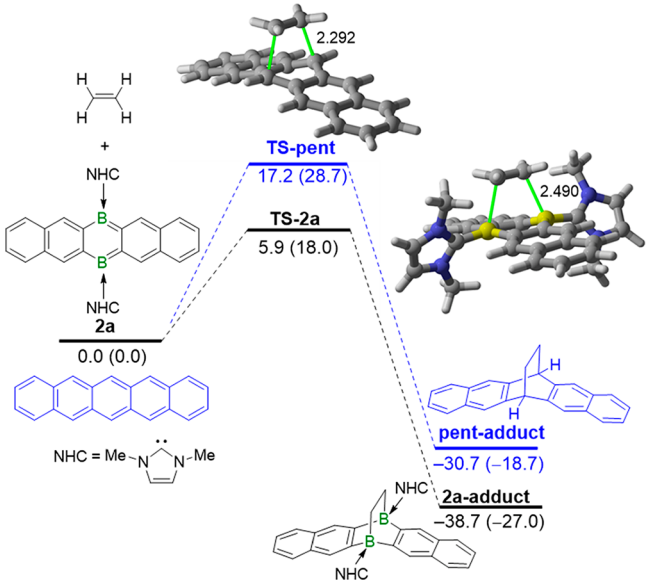

Figure 9. Computed reaction profiles for the cycloaddition reaction involving pentacene (blue lines) and borapentacene **2a** (black lines) with ethylene. Relative energies (free energies, computed at 298 K, within parentheses) and bond distances are given in kcal/mol and angstroms, respectively. All data have been computed at the PCM(benzene)-B3LYP-D3/def2-TZVPP//B3LYP-D3/def2-SVP level.

Information, the lower barrier of the **2a** and ethylene reaction originates solely from a more stabilizing interaction between the deformed reactants along the entire reaction coordinate, which comes from stronger dispersion, electrostatic, and orbital interactions, the latter of which once again contributes to a higher extent.

We applied the ASM-EDA method to understand in detail the computed further reactivity enhancement that results from the presence of additional fused aromatic rings in the system. To this end, we compared the cycloaddition reactions involving **1a**, **2a**, and ethylene. Figure 10a clearly indicates that the strain energy, that is, the energy required to deform the equilibrium geometry of the reactants along the process, is practically identical in both processes. Therefore, it is the interaction energy, which is more stabilizing for the reaction involving the larger B-doped PAH **2a** along the entire coordinate, that is the sole factor responsible for the lower barrier computed for the **2a** and ethylene reaction. According to the evolution of the EDA terms (Figure 10b), the higher interaction energy computed for the larger system is solely due to stronger orbital interactions, as the other contributors to the total interaction are nearly identical in both reactions. This is consistent with the further destabilization of the HOMO(π) in **2a** (−0.10 eV) in comparison to that in **1a** (−2.80 eV) as a consequence of the greater extension of the π-conjugation in the system, which results in a more favorable HOMO(diene)−LUMO(ethylene) gap and therefore a more stabilizing HOMO(diene) → LUMO(ethylene) orbital interaction.

CONCLUSIONS

Based on the results of the present computational study, it is confirmed that the CH/B replacement in anthracene has a dramatic impact on its Diels−Alder reactivity. Although the mechanism is identical, i.e., concerted through a highly synchronous transition state, boranthrene is much more reactive than anthracene from both kinetic and thermodynamic (by ca. 10 kcal/mol) points of view. This reactivity enhancement becomes particularly more evident in their reactions with CO_2, which is unfeasible for anthracene but proceeds with a relatively low barrier and in an exergonic transformation for the process involving boranthrene. According to the combination of the ASM and EDA methods, the enhanced reactivity of boranthrene as compared to anthracene solely originates from a stronger interaction between the deformed reactants along the entire reaction pathway. This can be ascribed to a significant enhancement of all the attractive interactions, namely, dispersion, electrostatic, and orbital interactions, the latter of which contributes to a much greater extent because the key HOMO(diene) → LUMO(dienophile) interaction becomes significantly more stabilizing for the process involving the B-doped system. We have studied the effect of additional fused rings in the PAH (pentacene and borapentacene) and found that the transformation becomes both kinetically (by ca. 4−5 kcal/mol) and thermodynamically (by ca. 12 kcal/mol) more favored with the increasing size of the system. This is exclusively due to stronger orbital interactions in the larger system, which significantly increase the total interaction between the reactants along the transformation. In our opinion, the insight gained in this work has contributed to rationalizing the physical factors

https://doi.org/10.1021/acsorginorgau.1c00023
ACS Org. Inorg. Au 2022, 2, 44−52

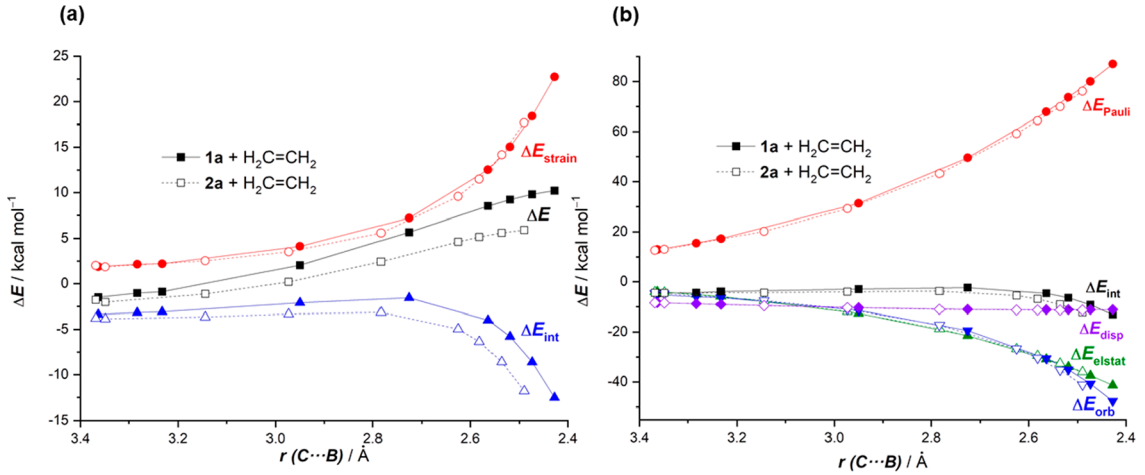

Figure 10. (a) Comparative activation strain and (b) energy decomposition analyses of the cycloaddition reactions between ethylene and boranthrene **1a** (solid lines) and borapentacene **2a** (dashed lines) projected onto the C···B bond-forming distance.

controlling the reactivity of B-doped PAHs and may stimulate future experiments toward the design of novel derivatives with tunable properties.

■ ASSOCIATED CONTENT

Supporting Information

The Supporting Information is available free of charge at https://pubs.acs.org/doi/10.1021/acsorginorgau.1c00023.

> Computed reaction profiles and individual strain energies, plot of the C···X bond-forming distance vs the computed free activation barrier, comparative activation strain analyses, and Cartesian coordinates and energies of all the species discussed in the text (PDF)

■ AUTHOR INFORMATION

Corresponding Author

Israel Fernández − *Departamento de Química Orgánica I and Centro de Innovación en Química Avanzada (ORFEO-CINQA), Faculdad de Ciencias Químicas, Universidad Complutense de Madrid, 28040 Madrid, Spain;* orcid.org/0000-0002-0186-9774; Email: israel@quim.ucm.es

Authors

Iván Cortés − *Facultad de Ciencias Bioquímicas y Farmacéuticas, Instituto de Química Rosario (IQUIR, CONICET-UNR), Universidad Nacional de Rosario, 2000 Rosario, Argentina*

Jorge Juan Cabrera-Trujillo − *Departamento de Química Orgánica I and Centro de Innovación en Química Avanzada (ORFEO-CINQA), Faculdad de Ciencias Químicas, Universidad Complutense de Madrid, 28040 Madrid, Spain;* orcid.org/0000-0002-1158-5409

Complete contact information is available at: https://pubs.acs.org/10.1021/acsorginorgau.1c00023

Notes

The authors declare no competing financial interest.

■ ACKNOWLEDGMENTS

This work was supported by the Spanish MICIIN (Grants PID2019-106184GB-I00 and RED2018-102387-T). I.C. acknowledges the Fundación Carolina and Ministerio de Educación de Argentina for a fellowship, and J.J.C-T. acknowledges the MINECO for a FPI grant.

■ REFERENCES

(1) Harvey, R. G. *Polycyclic Aromatic Hydrocarbons*; Wiley-VCH: Weinheim, Germany, 1997.

(2) *Polycyclic Arenes and Heteroarenes: Synthesis, Properties, and Applications*; Miao, Q., Ed.; Wiley-VCH: Weinheim, Germany, 2016.

(3) Anthony, J. E. Functionalized Acenes and Heteroacenes for Organic Electronics. *Chem. Rev.* **2006**, *106*, 5028−5048.

(4) Anthony, J. E. The Larger Acenes: Versatile Organic Semiconductors. *Angew. Chem., Int. Ed.* **2008**, *47*, 452−483.

(5) Wu, K. C.; Ku, P. J.; Lin, C. S.; Shih, H.-T.; Wu, F.-I.; Huang, M.-J.; Lin, J.-J.; Chen, I.-C.; Cheng, C.-H. The Photophysical Properties of Dipyrenylbenzenes and Their Application as Exceedingly Efficient Blue Emitters for Electroluminescent Devices. *Adv. Funct. Mater.* **2008**, *18*, 67−75.

(6) Omer, K. M.; Ku, S.-Y.; Wong, K.-T.; Bard, A. J. Efficient and Stable Blue Electrogenerated Chemiluminescence of Fluorene-Substituted Aromatic Hydrocarbons. *Angew. Chem., Int. Ed.* **2009**, *48*, 9300−9303.

(7) Lee, K. H.; Park, J. K.; Seo, J. H.; Park, S. W.; Kim, Y. S.; Kim, Y. K.; Yoon, S. S. Efficient deep-blue and white organic light-emitting diodes based on triphenylsilane-substituted anthracene derivatives. *J. Mater. Chem.* **2011**, *21*, 13640−13648.

(8) Xiao, J.; Liu, S.; Liu, Y.; Ji, L.; Liu, X.; Zhang, H.; Sun, X.; Zhang, Q. Synthesis, structure, and physical properties of 5,7,14,16-tetraphenyl-8:9,12:13-bisbenzo-hexatwistacene. *Chem. - Asian J.* **2012**, *7*, 561−564.

(9) Müllen, K.; Scherf, U. *Organic Light Emitting Devices: Synthesis, Properties and Applications*; Wiley-VCH: Weinheim, Germany, 2006.

(10) Bendikov, M.; Wudl, F.; Perepichka, D. F. Tetrathiafulvalenes, Oligoacenenes, and Their Buckminsterfullerene Derivatives: The Brick and Mortar of Organic Electronics. *Chem. Rev.* **2004**, *104*, 4891−4946.

(11) Zhan, X.; Zhang, J.; Tang, S.; Lin, Y.; Zhao, M.; Yang, J.; Zhang, H.-L.; Peng, Q.; Yu, G.; Li, Z. Pyrene fused perylene diimides: synthesis, characterization and applications in organic field-effect transistors and optical limiting with high performance. *Chem. Commun.* **2015**, *51*, 7156−7159.

(12) Li, C.; Wang, Y.; Zhang, T.; Zheng, B.; Xu, J.; Miao, Q. Tertiary Amines Differentiated from Primary and Secondary Amines by Active

Ester-Functionalized Hexabenzoperylene in Field Effect Transistors. *Chem. - Asian J.* **2019**, *14*, 1676−1680.
(13) Liu, G.; Xiao, C.; Negri, F.; Li, Y.; Wang, Z. Dodecatwistarene Imides with Zigzag-Twisted Conformation for Organic Electronics. *Angew. Chem., Int. Ed.* **2020**, *59*, 2008−2012.
(14) Tremblay, N. J.; Gorodetsky, A. A.; Cox, M. P.; Schiros, T.; Kim, B.; Steiner, R.; Bullard, Z.; Sattler, A.; So, W.-H.; Itoh, Y.; Toney, M. F.; Ogasawara, H.; Ramirez, A. P.; Kymissis, I.; Steigerwald, M. L.; Nuckolls, C. Photovoltaic Universal Joints: Ball-and-Socket Interfaces in Molecular Photovoltaic Cells. *ChemPhysChem* **2010**, *11*, 799−803.
(15) Xiao, S.; Kang, S. J.; Wu, Y.; Ahn, S.; Kim, J. B.; Loo, Y.-L.; Siegrist, T.; Steigerwald, M. L.; Li, H.; Nuckolls, C. Supersized contorted aromatics. *Chem. Sci.* **2013**, *4*, 2018−2023.
(16) Brabec, C.; Scherf, U.; Dyakonov, V. *Organic Photovoltaics-Materials, Device Physics, and Manufacturing Technologies*, 2nd ed.; Wiley-VCH: Weinheim, Germany, 2014.
(17) De Angelis, F.; Gaspari, M.; Procopio, A.; Cuda, G.; Di Fabrizio, E. Direct mass spectrometry investigation on Pentacene thin film oxidation upon exposure to air. *Chem. Phys. Lett.* **2009**, *468*, 193−196.
(18) Bénard, C. P.; Geng, Z.; Heuft, M. A.; VanCrey, K.; Fallis, A. G. Double Diels−Alder Strategies to Soluble 2,9- and 2,9,6,13-Tetraethynylpentacenes, Photolytic [4 + 4] Cycloadditions, and Pentacene Crystal Packing. *J. Org. Chem.* **2007**, *72*, 7229−7236.
(19) Stępień, M.; Gońka, E.; Żyła, M.; Sprutta, N. Heterocyclic Nanographenes and Other Polycyclic Heteroaromatic Compounds: Synthetic Routes, Properties, and Applications. *Chem. Rev.* **2017**, *117*, 3479−3716.
(20) Hirai, M.; Tanaka, N.; Sakai, M.; Yamaguchi, S. Structurally Constrained Boron-, Nitrogen-, Silicon-, and Phosphorus-Centered Polycyclic π-Conjugated Systems. *Chem. Rev.* **2019**, *119*, 8291−8331.
(21) Bunz, U. H. F.; Freudenberg, J. N-Heteroacenes and N-Heteroarenes as N-Nanocarbon Segments. *Acc. Chem. Res.* **2019**, *52*, 1575−1587.
(22) Entwistle, C. D.; Marder, T. B. Boron Chemistry Lights the Way: Optical Properties of Molecular and Polymeric Systems. *Angew. Chem., Int. Ed.* **2002**, *41*, 2927−2931.
(23) Entwistle, C. D.; Marder, T. B. Applications of Three-Coordinate Organoboron Compounds and Polymers in Optoelectronics. *Chem. Mater.* **2004**, *16*, 4574−4585.
(24) Jäkle, F. Lewis acidic organoboron polymers. *Coord. Chem. Rev.* **2006**, *250*, 1107−1121.
(25) Yamaguchi, S.; Wakamiya, A. Boron as a key component for new π-electron materials. *Pure Appl. Chem.* **2006**, *78*, 1413−1424.
(26) Jäkle, F. Advances in the synthesis of organoborane polymers for optical, electronic, and sensory applications. *Chem. Rev.* **2010**, *110*, 3985−4022.
(27) Lorbach, A.; Bolte, M.; Li, H.; Lerner, H.-W.; Holthausen, M. C.; Jäkle, F.; Wagner, M. 9,10-Dihydro-9,10-diboraanthracene: Supramolecular Structure and Use as a Building Block for Luminescent Conjugated Polymers. *Angew. Chem., Int. Ed.* **2009**, *48*, 4584−4588.
(28) Lorbach, A.; Bolte, M.; Lerner, H.-W.; Wagner, M. Lewis-base adducts of 9,10-dihydro-9,10-diboraanthracene: ditopic hydroboration reagents and a B−N analogue of triptycene. *Chem. Commun.* **2010**, *46*, 3592−3594.
(29) Hoffend, C.; Schödel, F.; Bolte, M.; Lerner, H.-W.; Wagner, M. Boron-Doped Tri(9,10-anthrylene)s: Synthesis, Structural Characterization, and Optoelectronic Properties. *Chem. - Eur. J.* **2012**, *18*, 15394−15405.
(30) Reus, C.; Weidlich, S.; Bolte, M.; Lerner, H.-W.; Wagner, M. C-Functionalized, Air- and Water-Stable 9,10-Dihydro-9,10-diboraanthracenes: Efficient Blue to Red Emitting Luminophores. *J. Am. Chem. Soc.* **2013**, *135*, 12892−12907.
(31) von Grotthuss, E.; Diefenbach, M.; Bolte, M.; Lerner, H.-W.; Holthausen, M. C.; Wagner, M. Reversible Dihydrogen Activation by Reduced Aryl Boranes as Main-Group Ambiphiles. *Angew. Chem., Int. Ed.* **2016**, *55*, 14067−14071.
(32) Taylor, J. W.; McSkimming, A.; Guzman, C. F.; Harman, W. H. N-Heterocyclic Carbene-Stabilized Boranthrene as a Metal-Free Platform for the Activation of Small Molecules. *J. Am. Chem. Soc.* **2017**, *139*, 11032−11035.
(33) Fernández, I.; Bickelhaupt, F. M. The Activation Strain Model and Molecular Orbital Theory: Understanding and Designing Chemical Reactions. *Chem. Soc. Rev.* **2014**, *43*, 4953−4967.
(34) Bickelhaupt, F. M.; Houk, K. N. Analyzing Reaction Rates with the Distortion/Interaction-Activation Strain Model. *Angew. Chem., Int. Ed.* **2017**, *56*, 10070−10086.
(35) Vermeeren, P.; Hamlin, T. A.; Bickelhaupt, F. M. Chemical reactivity from an activation strain perspective. *Chem. Commun.* **2021**, *57*, 5880−5896.
(36) See also: Fernández, F. Understanding Trends in Reaction Barriers. In *Discovering the Future of Molecular Sciences*; Pignataro, B., Ed.; Wiley-VCH: Weinheim, Germany, 2014; pp 165−187.
(37) Bickelhaupt, F. M.; Baerends, E. J. Kohn-Sham Density Functional Theory: Predicting and Understanding Chemistry. In *Reviews in Computational Chemistry*, Vol. *15*; Lipkowitz, K. B., Boyd, D. B., Eds.; Wiley-VCH: New York, NY, 2000; pp 1−86.
(38) Zhao, L.; von Hopffgarten, M.; Andrada, D. M.; Frenking, G. Energy Decomposition Analysis. *Wiley Interdiscip. Rev.: Comput. Mol. Sci.* **2018**, *8*, e1345.
(39) Fernández, I. Energy Decomposition Analysis and Related Methods. In *Applied Theoretical Organic Chemistry*; Tantillo, D. J., Ed.; World Scientific: Hackensack, NJ, 2018; pp 191−226.
(40) Chen, S.; Huang, X.; Meggers, E.; Houk, K. N. Origins of Enantioselectivity in Asymmetric Radical Additions to Octahedral Chiral-at-Rhodium Enolates: A Computational Study. *J. Am. Chem. Soc.* **2017**, *139*, 17902−17907.
(41) Hamlin, T. A.; Levandowski, B. J.; Narsaria, A. K.; Houk, K. N.; Bickelhaupt, F. M. Structural Distortion of Cycloalkynes Influences Cycloaddition Rates both by Strain and Interaction Energies. *Chem. - Eur. J.* **2019**, *25*, 6342−6348.
(42) Kamber, D. N.; Nguyen, S. S.; Liu, F.; Briggs, J. S.; Shih, H.-W.; Row, R. D.; Long, Z. G.; Houk, K. N.; Liang, Y.; Prescher, J. A. Isomeric triazines exhibit unique profiles of bioorthogonal reactivity. *Chem. Sci.* **2019**, *10*, 9109−9114.
(43) Hamlin, T.; Fernández, I.; Bickelhaupt, F. M. How Dihalogens Catalyze Michael Addition Reactions. *Angew. Chem., Int. Ed.* **2019**, *58*, 8922−8926.
(44) Couce-Rios, A.; Lledós, A.; Fernández, I.; Ujaque, G. Origin of the Anti-Markovnikov Hydroamination of Alkenes Catalyzed by L−Au(I) Complexes: Coordination Mode Determines Regioselectivity. *ACS Catal.* **2019**, *9*, 848−858.
(45) Vermeeren, P.; Hamlin, T. A.; Fernández, I.; Bickelhaupt, F. M. How Lewis Acids Catalyze Diels−Alder Reactions. *Angew. Chem., Int. Ed.* **2020**, *59*, 6201−6206.
(46) Hamlin, T. A.; Bickelhaupt, F. M.; Fernández, I. The Pauli Repulsion-Lowering Concept in Catalysis. *Acc. Chem. Res.* **2021**, *54*, 1972−1981.
(47) García-Rodeja, Y.; Solá, M.; Fernández, I. Understanding the Reactivity of Planar Polycyclic Aromatic Hydrocarbons: Towards the Graphene Limit. *Chem. - Eur. J.* **2016**, *22*, 10572−10580.
(48) García-Rodeja, Y.; Solá, M.; Bickelhaupt, F. M.; Fernández, I. Reactivity and Selectivity of Bowl-Shaped Polycyclic Aromatic Hydrocarbons: Relationship to C_{60}. *Chem. - Eur. J.* **2016**, *22*, 1368−1378.
(49) García-Rodeja, Y.; Fernández, I. Factors Governing the Diels−Alder Reactivity of (2,7)Pyrenophanes. *J. Org. Chem.* **2017**, *82*, 8157−8164.
(50) García-Rodeja, Y.; Fernández, I. Influence of the Transition-Metal Fragment on the Reactivity of Metallaanthracenes. *Chem. - Eur. J.* **2017**, *23*, 6634−6642.
(51) García-Rodeja, Y.; Fernández, I. Impact of C = C/B-N Replacement on the Diels−Alder Reactivity of Curved Polycyclic Aromatic Hydrocarbons. *Chem. - Eur. J.* **2019**, *25*, 9771−9779.

https://doi.org/10.1021/acsorginorgau.1c00023
ACS Org. Inorg. Au 2022, 2, 44−52

(52) See also: Fernández, I. Understanding the reactivity of polycyclic aromatic hydrocarbons and related compounds. *Chem. Sci.* **2020**, *11*, 3769−3779.
(53) Frisch, M. J.; Trucks, G. W.; Schlegel, H. B.; Scuseria, G. E.; Robb, M. A.; Cheeseman, J. R.; Scalmani, G.; Barone, V.; Mennucci, B.; Petersson, G. A.; Nakatsuji, H.; Caricato, M.; Li, X.; Hratchian, H. P.; Izmaylov, A. F.; Bloino, J.; Zheng, G.; Sonnenberg, J. L.; Hada, M.; Ehara, M.; Toyota, K.; Fukuda, R.; Hasegawa, J.; Ishida, M.; Nakajima, T.; Honda, Y.; Kitao, O.; Nakai, H.; Vreven, T.; Montgomery, J. A., Jr.; Peralta, J. E.; Ogliaro, F.; Bearpark, M.; Heyd, J. J.; Brothers, E.; Kudin, K. N.; Staroverov, V. N.; Kobayashi, R.; Normand, J.; Raghavachari, K.; Rendell, A.; Burant, J. C.; Iyengar, S. S.; Tomasi, J.; Cossi, M.; Rega, N.; Millam, J. M.; Klene, M.; Knox, J. E.; Cross, J. B.; Bakken, V.; Adamo, C.; Jaramillo, J.; Gomperts, R.; Stratmann, R. E.; Yazyev, O.; Austin, A. J.; Cammi, R.; Pomelli, C.; Ochterski, J. W.; Martin, R. L.; Morokuma, K.; Zakrzewski, V. G.; Voth, G. A.; Salvador, P.; Dannenberg, J. J.; Dapprich, S.; Daniels, A. D.; Farkas, Ö.; Foresman, J. B.; Ortiz, J. V.; Cioslowski, J.; Fox, D. J. *Gaussian 09*, rev. D.01; Gaussian, Inc.: Wallingford, CT, 2009.
(54) Becke, A. D. Density-functional thermochemistry. III. The role of exact exchange. *J. Chem. Phys.* **1993**, *98*, 5648−5652.
(55) Lee, C.; Yang, W.; Parr, R. G. Development of the Colle-Salvetti correlation-energy formula into a functional of the electron density. *Phys. Rev. B: Condens. Matter Mater. Phys.* **1988**, *37*, 785−789.
(56) Vosko, S. H.; Wilk, L.; Nusair, M. Accurate spin-dependent electron liquid correlation energies for local spin density calculations: a critical analysis. *Can. J. Phys.* **1980**, *58*, 1200−1211.
(57) Grimme, S.; Antony, J.; Ehrlich, S.; Krieg, H. A consistent and accurate ab initio parametrization of density functional dispersion correction (DFT-D) for the 94 elements H-Pu. *J. Chem. Phys.* **2010**, *132*, 154104−15419.
(58) Weigend, F.; Ahlrichs, R. Balanced basis sets of split valence, triple zeta valence and quadruple zeta valence quality for H to Rn: Design and assessment of accuracy. *Phys. Chem. Chem. Phys.* **2005**, *7*, 3297−3305.
(59) Weigend, F. Accurate Coulomb-fitting basis sets for H to Rn. *Phys. Chem. Chem. Phys.* **2006**, *8*, 1057−1065.
(60) Gonzalez, C.; Schlegel, H. B. Reaction path following in mass-weighted internal coordinates. *J. Phys. Chem.* **1990**, *94*, 5523−5527.
(61) Miertuš, S.; Scrocco, E.; Tomasi, J. Electrostatic interaction of a solute with a continuum. A direct utilization of ab-initio molecular potentials for the prevision of solvent effects. *Chem. Phys.* **1981**, *55*, 117−129.
(62) Pascual-Ahuir, J. L.; Silla, E.; Tuñón, I. GEPOL: An improved description of molecular surfaces. III. A new algorithm for the computation of a solvent-excluding surface. *J. Comput. Chem.* **1994**, *15*, 1127−1138.
(63) Barone, V.; Cossi, M. Quantum Calculation of Molecular Energies and Energy Gradients in Solution by a Conductor Solvent Model. *J. Phys. Chem. A* **1998**, *102*, 1995−2001.
(64) Mitoraj, M. P.; Michalak, A.; Ziegler, T. A Combined Charge and Energy Decomposition Scheme for Bond Analysis. *J. Chem. Theory Comput.* **2009**, *5*, 962−975.
(65) te Velde, G.; Bickelhaupt, F. M.; Baerends, E. J.; Fonseca Guerra, C.; van Gisbergen, S. J. A.; Snijders, J. G.; Ziegler, T. Chemistry with ADF. *J. Comput. Chem.* **2001**, *22*, 931−967.
(66) .Baerends, E. J.; Ziegler, T.; Atkins, A. J.; Autschbach, J.; Baseggio, O.; Bashford, D.; Bérces, A.; Bickelhaupt, F. M.; Bo, C.; Boerrigter, P. M.; Cappelli, C.; Cavallo, L.; Daul, C.; Chong, D. P.; Chulhai, D. V.; Deng, L.; Dickson, R. M.; Dieterich, J. M.; Egidi, F.; Ellis, D. E.; van Faassen, M.; Fan, L.; Fischer, T. H.; Förster, A.; Fonseca Guerra, C.; Franchini, M.; Ghysels, A.; Giammona, A.; van Gisbergen, S. J. A.; Goez, A.; Götz, A. W.; Groeneveld, J. A.; Gritsenko, O. V.; Grüning, M.; Gusarov, S.; Harris, F. E.; van den Hoek, P.; Hu, Z.; Jacob, C. R.; Jacobsen, H.; Jensen, L.; Joubert, L.; Kaminski, J. W.; van Kessel, G.; König, C.; Kootstra, F.; Kovalenko, A.; Krykunov, M. V.; Lafiosca, P.; van Lenthe, E.; McCormack, D. A.; Medves, M.; Michalak, A.; Mitoraj, M.; Morton, S. M; Neugebauer, J.; Nicu, V. P.; Noodleman, L.; Osinga, V. P.; Patchkovskii, S.; Pavanello, M.; Peeples, C. A.; Philipsen, P. H. T.; Post, D.; Pye, C. C.; Ramanantoanina, H.; Ramos, P.; Ravenek, W.; Reimann, M.; Rodríguez, J. I.; Ros, P.; Rüger, R.; Schipper, P. R. T.; Schlüns, D.; van Schoot, H.; Schreckenbach, G.; Seldenthuis, J. S.; Seth, M.; Snijders, J. G.; Solà, M.; Stener, M.; Swart, M.; Swerhone, D.; Tognetti, V.; te Velde, G.; Vernooijs, P.; Versluis, L.; Visscher, L.; Visser, O.; Wang, F.; Wesolowski, T. A.; van Wezenbeek, E. M.; Wiesenekker, G.; Wolff, S. K.; Woo, T. K.; Yakovlev, A. L. *ADF 2020*; Vrije Universiteit: Amsterdam, The Netherlands, 2020.
(67) Snijders, J. G.; Vernooijs, P.; Baerends, E. J. Roothaan-Hartree-Fock-Slater Atomic Wave Functions. Single-Zeta, Double-Zeta, and Extended Slater-Type Basis Sets for ^{87}Fr-^{103}Lr. *At. Data Nucl. Data Tables* **1981**, *26*, 483−509.
(68) Krijn, J.; Baerends, E. J. *Fit Functions in the HFS-Method: Internal Report*; Vrije Universiteit: Amsterdam, Netherlands, 1984.
(69) van Lenthe, E.; Baerends, E. J.; Snijders, J. G. Relativistic regular two-component Hamiltonians. *J. Chem. Phys.* **1993**, *99*, 4597−4610.
(70) van Lenthe, E.; Baerends, E. J.; Snijders, J. G. Relativistic total energy using regular approximations. *J. Chem. Phys.* **1994**, *101*, 9783−9792.
(71) van Lenthe, E.; Ehlers, A.; Baerends, E. J. Geometry optimizations in the zero order regular approximation for relativistic effects. *J. Chem. Phys.* **1999**, *110*, 8943−8953.
(72) A similar reactivity trend was found at the accurate PCM(benzene)-M06-2X/def2-TZVPP//M06-2X/def2-SVP level. For the cycloaddition reactions involving anthracene and boranthrene **1a**, a $\Delta\Delta G^{\ddagger}$ value of 11.3 kcal/mol was computed, which was nearly identical to that computed at the PCM(benzene)-B3LYP-D3/def2-TZVPP//B3LYP-D3/def2-SVP level ($\Delta\Delta G^{\ddagger}$ = 11.5 kcal/mol, see Figure 2).
(73) Fernández, I. Understanding the Reactivity of Fullerenes through the Activation Strain Model. *Eur. J. Org. Chem.* **2018**, *2018*, 1394−1402.
(74) Fernández, I. Combined activation strain model and energy decomposition analysis methods: a new way to understand pericyclic reactions. *Phys. Chem. Chem. Phys.* **2014**, *16*, 7662−7671.
(75) The difference in the electrostatic interactions, although less significant, may be ascribed to the difference in the electronegativity of boron and carbon atoms, which makes the reactive B═C bonds in boranthrene much more polar than the C═C bonds in anthracene.
(76) Performing this analysis at a consistent point along the reaction coordinate (near all transition structures), rather than at the transition state alone, ensures that the energy values are not skewed by the position of the transition state on the potential energy surface. See reference 13 for further details.
(77) For a plot of the individual contributions to the total strain energies, see Figure S2 in the Supporting Information.
(78) Schleyer, P. v. R.; Manoharan, M.; Jiao, H.; Stahl, F. The Acenes: Is There a Relationship between Aromatic Stabilization and Reactivity? *Org. Lett.* **2001**, *3*, 3643−3646.
(79) Leffler, J. E. Parameters for the Description of Transition States. *Science* **1953**, *117*, 340−341.
(80) Hammond, G. S. A Correlation of Reaction Rates. *J. Am. Chem. Soc.* **1955**, *77*, 334−338.

https://doi.org/10.1021/acsorginorgau.1c00023
ACS Org. Inorg. Au 2022, 2, 44−52